

A Heterogeneous Chiplet Architecture for Accelerating End-to-End Transformer Models

Harsh Sharma*

Washington State University, Pullman, WA, USA, harsh.sharma@wsu.edu

Pratyush Dhingra

Washington State University, Pullman, WA, USA, pratyush.dhingra@wsu.edu

Janardhan Rao Doppa

Washington State University, Pullman, WA, USA, doppa@wsu.edu

Umit Y. Ogras

University of Wisconsin Madison, Madison, WI, USA, uogras@wisc.edu

Partha Pratim Pande

Washington State University, Pullman, WA, USA, pande@wsu.edu

Transformers have revolutionized deep learning and generative modeling, enabling unprecedented advancements in natural language processing tasks. However, the size of transformer models is increasing continuously, driven by enhanced capabilities across various deep learning tasks. This trend of ever-increasing model size has given rise to new challenges in terms of memory and compute requirements. Conventional computing platforms, including GPUs, suffer from suboptimal performance due to the memory demands imposed by the models with millions/billions of parameters. The emerging chiplet-based platforms provide a new avenue for compute- and data-intensive machine learning (ML) applications enabled by a Network-on-Interposer (NoI). However, designing suitable hardware accelerators for executing Transformer inference workloads is challenging due to a wide variety of complex computing kernels in the Transformer architecture. In this paper, we leverage chiplet-based heterogeneous integration (HI) to design a high-performance and energy-efficient multi-chiplet platform to accelerate transformer workloads. We demonstrate that the proposed NoI architecture caters to the data access patterns inherent in a transformer model. The optimized placement of the chiplets and the associated NoI links and routers enable superior performance compared to the state-of-the-art hardware accelerators. The proposed NoI-based architecture demonstrates scalability across varying transformer models and improves latency and energy efficiency by up to 22.8× and 5.36×, respectively.

CONCEPTS • 2.5D • NLP • Processing-in-memory • Network-on-interposer • Transformer • Chiplet-based architecture

* Authors' addresses: Harsh Sharma, harsh.sharma@wsu.edu, Washington State University, School of Electrical Engineering and Computer Science, Pullman, WA, 99163, USA; Pratyush Dhingra, pratyush.dhingra@wsu.edu, Washington State University, School of Electrical Engineering and Computer Science, Pullman, WA, 99163, USA; Janardhan Rao Doppa, doppa@wsu.edu, Washington State University, School of Electrical Engineering and Computer Science, Pullman, WA, 99163, USA; Umit Y. Ogras, uogras@wisc.edu, University of Wisconsin-Madison, Department of Electrical and Computer Engineering, Madison, WI, 53706, USA; Partha Pratim Pande, pande@wsu.edu, Washington State University, School of Electrical Engineering and Computer Science, Pullman, WA, 99163, USA.

1 INTRODUCTION

We are at the cusp of a revolution from deep generative AI models, also referred to as *foundation models (FMs)*, for text (e.g., ChatGPT) and images (e.g., stable diffusion) with hundreds of billions of parameters trained on a massive amount of unlabeled data. In the future, fine-tuning FMs on domain-specific private data (e.g., BloombergGPT for finance, AutoGPT for general-purpose automation) to solve a specific task with high accuracy will emerge as a fundamental challenge. The current FMs employ Transformer architectures due to their widespread success in applications, including natural language processing, computer vision, and multi-modal integration [1] [2]. The number of parameters and complexity of transformer models are growing at a rapid pace to meet the application demands, including scale of data and high accuracy. Hence, designing suitable hardware accelerators for Transformer models involves significant computation and storage challenges, particularly when addressing longer contextual information. The main challenge arises from the quadratic relationship between the compute requirements and the input sequence length (N). Unlike recurrent neural networks (RNNs), Transformers employ self-attention to process various modalities of data, including text, images, videos, and speech, enabling tokens within sequences to relate to one another effectively. This approach overcomes the vanishing gradient problem in RNNs and allows to effectively leverage long-range sequential dependencies.

Widespread adoption of Transformer models in real-world applications implies a vast demand for designing hardware platforms with adequate computational and storage resources [1] [2] [3]. We must tackle complex data movement, memory hierarchy, and latency challenges while designing suitable hardware architectures. Hence, there is a need for designing large-scale chips with high memory and compute capabilities. Moreover, due to various types of computational kernels involved in Transformer models, we require different types of processing elements, such as Tensor cores, GPUs, DRAMs, and processing-in-memory (PIM)-based accelerators on the same system. Such large-scale and heterogeneous integration increases the area of monolithic chips significantly [4]. One of the major challenges in the silicon industry is the exploding fabrication cost as the size of monolithic chips approaches the reticle limit [4].

Chiplet-based 2.5D systems that integrate multiple smaller chips (chiplets) on a single interposer offer a promising solution for reducing the manufacturing cost of large monolithic chips and enabling large-scale heterogeneous integration in a single system. Chiplets are connected through the network-on-interposer (NoI). In a heterogeneous chiplet-based system, designing a scalable NoI architecture is daunting due to the relatively large physical distances between chiplets, poor technology scaling of electrical wires, and varying data movement patterns depending on the heterogeneity in constituent chiplets. This data movement introduces performance overhead. In addition, managing data movement across different levels of the memory hierarchy is non-trivial, requiring careful placement of chiplets, NoI links, and routers to ensure efficient data access paths. However, current state-of-the-art Transformer accelerators do not consider the challenges associated with the heterogeneous integration (HI) within a single system. We adopt a holistic view by considering the interactions among various computing kernels within transformers to design the HI architecture. We also optimize the system-level performance by choosing a suitable chiplet configuration for each computational kernel. In this paper, we present an NoI backbone design methodology, enabling a heterogeneous chiplet architecture for end-to-end acceleration of Transformer models, and demonstrate significant improvements over existing hardware accelerators.

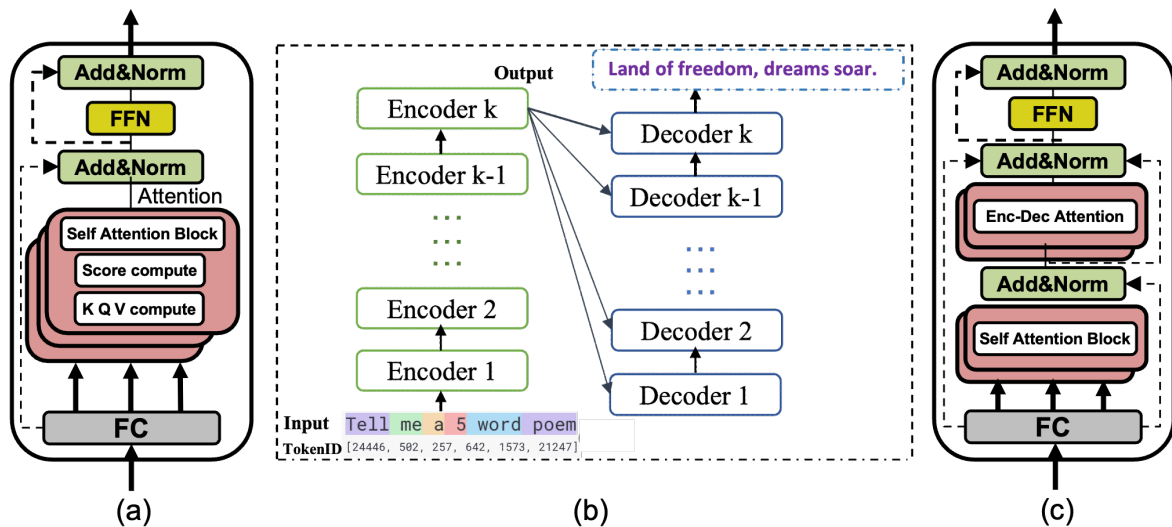


Fig. 1: Overview of the Transformer model; (a) Encoder structure and inherent computational kernels; (b) overall dataflow structure (c) Decoder structure with their inherent computational kernels.

The major contributions of this paper are as follows:

1. We propose a novel methodology for designing a high-performance and energy-efficient NoI architecture supporting heterogeneous chiplets for accelerating Transformer models.
2. We demonstrate that the proposed NoI architecture caters to the data access patterns inherent in a heterogeneous system. The optimized placement of the chiplets and the associated NoI links and routers enable superior performance compared to the state-of-the-art counterparts.
3. Extensive performance evaluation shows up to $22.8\times$ and $5.36\times$ reduction in latency and energy compared to state-of-the-art 2.5D designs.

The rest of the paper is organized as follows. Section II presents the relevant prior work. Section III introduces the overall architecture and explains the associated data flow. Section IV presents the experimental setup and detailed performance evaluation. Finally, Section V concludes the paper by highlighting the salient contributions of this work.

2 RELATED WORK

As this work is focused on designing 2.5D accelerators for Transformers, we review the related work in two parts: 2.5D-based manycore architectures and Transformer accelerators.

2.5D-based manycore architectures: Both application-specific and general-purpose chiplet architectures have been explored. Design space exploration of 2.5D-based systems considering technology nodes, chiplet-sizes, big-little chiplet paradigm, and multi-link network frequency architectures have been proposed [5] [6] [7] [8]. The NoI paradigm becomes crucial as the communication demand increases with many chiplets integrated on the same substrate [5]. So far, multiple NoI architectures have been proposed in the literature. Most of these architectures are based on conventional multi-hop interconnection architectures, such as mesh or torus [6]. A server-scale application-specific 2.5D architecture called SWAP is proposed for deep learning workloads [9]. SIMBA introduces tiling optimizations on fixed NoI topologies for executing deep models such as ResNet50 [10]. NN-Baton proposes a framework to explore the chiplet design space for convolutional operations [11]. Recent work discusses the advantages of integrating heterogeneous chiplets on the interposer to reduce

design costs [12]. A scalable high-performance chiplet-based architecture called Hexamesh has been proposed recently [13]. However, *none of the above 2.5D architecture can be employed off-the-shelf to accelerate Transformer models* as they cannot handle the data-access patterns involving heterogeneous chiplets and computational kernels.

Transformer accelerators: PIM is an enabling technology to accelerate deep learning workloads [9]. Several PIM architectures have been proposed for Transformer models. ReTransformer is a ReRAM-based PIM accelerator designed only for the attention kernel and is oblivious to the data access patterns involved in a Transformer model [1]. Additionally, the expected rewrites due to intermediate results during the attention computation within the Transformer model would exceed the write endurance of the ReRAM blocks. We have quantified this limitation in the section 4.4. Xformer is another accelerator that uses ReRAM-SRAM arrays to divide the attention kernel into dynamic and static components, respectively [14]. Xformer maps more frequently updated computation kernels to SRAM arrays. HAIMA is a recently proposed hybrid DRAM-SRAM compute-in-memory architecture [3]. HAIMA accelerates parallel kernels using SRAM and DRAM components. Multiple ASIC designs have been proposed to accelerate the attention kernel only [15] [16] [17]. These ASICs do not accelerate the entire Transformer model. EdgeBERT leverages dynamic voltage-frequency scaling based on the early exit prediction of ALBERT, which is a lightweight Transformer model with reduced memory footprint [18]. A recently proposed monolithic-3D accelerator, called AccelTran prunes activations at runtime [19]. TransCODE is another codesign framework that finds a Transformer-accelerator pair that maximizes the performance objectives within the given user-defined constraints [20]. Newton, FIMDRAM, and McDRAM cascade bit-arithmetic units to do computation near DRAM banks [17] [21]. However, the complicated bit-parallel and bulky buffers incur significant overhead and decrease memory density. Other methodologies, such as TurboTransformer, introduce large area overhead and have limited acceleration due to simpler tiled computation [22]. TransPIM implements the computing kernels in HBM memory stacks with optimized data paths using token sharing in a ring broadcast among memory banks during attention computation. TransPIM uses auxiliary compute units to avoid extra data movement and suffers from latency overhead at each kernel, compromising the overall execution time [2].

To summarize, *previous work primarily focuses on accelerating the attention kernel only*. Moreover, none of the prior work considers the role of heterogeneous chiplets along with the associated dataflow to accelerate end-to-end Transformer models. In this paper, we fill this critically important gap in the state-of-art by proposing design principles of a heterogeneous chiplet-based 2.5D manycore architecture to accelerate end-to-end Transformer models.

3 TRANSFORMER COMPUTATION KERNELS

This section presents the distinct features of a Transformer model and explains the computational and communication characteristics during the inference process.

3.1 Computational Kernels within Transformers

A Transformer primarily comprises an encoder and a decoder stack with a similar structure. The computational structure is identical in Transformer models with varying numbers of encoders/decoder blocks. Figures 1 show the encoder-decoder structure with their internal computational blocks: it takes an input sequence of length N (e.g., natural text), then it produces an output sequence (e.g., natural text). The encoder has a stack of k identical blocks. Each block consists of two major functional modules: multi-head self-attention and feed-forward (FF). Following these two functional modules, there is a residual block to add the input and the output and to perform the layer norm operation. The multi-head attention layer receives data from the input embedding or previous encoder block. The decoder stack also consists of k identical blocks with an extra cross-attention layer to connect with the output from the last encoder stack.

A Transformer initiates the computation by loading the word embedding H_{emb} and positional encodings P_{enc} . Tokenization is the matrix-vector multiplication (MVM) process, where an embedding layer first processes inputs (e.g., words in a sentence) to obtain a learned vector representation of each word in the input sequence. This is a one-time process for an entire Transformer model (encoder-decoder stack).

$$H = H_{emb} + P_{enc}(H_{emb}) \quad (1)$$

After the tokenizing step (a linear MVM operation), each token is represented by a vector of length d_{model} , where d_{model} depends on the hidden dimension of the Transformer (e.g., $d_{model} = 128$ for BERT-Tiny and $d_{model} = 768$ for BERT-Base) [20]. The corresponding MVM operation is weight stationary and can be effectively computed using processing-in-memory (PIM)-based compute units such as ReRAM chipllets. Next, the weight matrices for the multi-head attention operations are loaded from the memory to the compute units (the structure of each compute unit corresponding to the kernel is explained later). Consistent with the prior work, for h multi heads (each represented with a 16-bit floating point), h separate weight matrices must be loaded to compute Q_i, K_i, V_i shown in (3):

$$\text{load } W_i^Q, W_i^K, \text{ and } W_i^V \in \mathbb{R}^{\frac{d_{model} \times d_{model}}{h}} \quad (2)$$

$$Q_i, K_i, V_i = HW_i^Q, HW_i^K, HW_i^V \quad \forall i \in N \quad (3)$$

Within each self-attention head, the generated tokens are multiplied by distinct weight matrices (distinct for h heads) to obtain the Query Q , Key K , and Value V matrices (3). For each sequence, the attention generates a representation of the sequence encoded with weighted information from all (or a subset in Masked-Attention) other tokens. This computation depends on the size of the W_Q , W_K , and W_V matrices. For every self-attention layer within a Transformer encoder, all the compute units must be rewritten before the MVM operation is performed since the *inputs change dynamically for each token* and must be stored in internal registers or on-chip buffers. Traditionally, crossbar-based PIM platforms are employed for the MVM operations involved in DNN workloads [9]. In this case, however, such intermediate matrices will require substantial storage capacity or frequent updates. Hence, traditional nonvolatile memory (NVM)-based PIM architectures are unsuitable here due to their limited write endurance [23]. For example, for BERT-Base and Bert-Tiny, intermediate matrices take up to $8.98\times$ and $2.06\times$ of original weight matrix storage, respectively. The total memory requirements for the two models are 52.8MB and 3.4GB, respectively, when only the weights and positional embeddings are stored [20]. This storage will grow even more for bigger models, which cannot be stored by using more resources and by remaining within the reticle limit of the 2.5D system with an acceptable yield. Hence, the only possibility is to update these intermediate matrices continuously. Consequently, the memory rewrite easily crosses the acceptable endurance limit of the PIM devices [23]. Hence, to implement the attention computation, instead of PIM chipllets, we use the streaming multiprocessors (SMs) along with the associated memory controllers (MCs) to access the weights W from the DRAM chipllet. All the K, Q, V computations are executed parallelly, leading to a many-to-few traffic scenario (multiple SMs and a few MCs).

Next, the outputs, Query, and Key matrices are multiplied and normalized with a hidden dimension d_{model} by a Softmax layer to generate the intermediate attention probabilities (4) & (5).

$$\alpha_i = Q_i K_i \quad (4)$$

$$Score_i = softmax\left(\frac{\alpha_i}{\sqrt{d_{model}}}\right) \quad (5)$$

The intermediate attention probabilities are then multiplied with the Value matrix to obtain the final output (6).

$$P_i = Score_i V_i \quad (6)$$

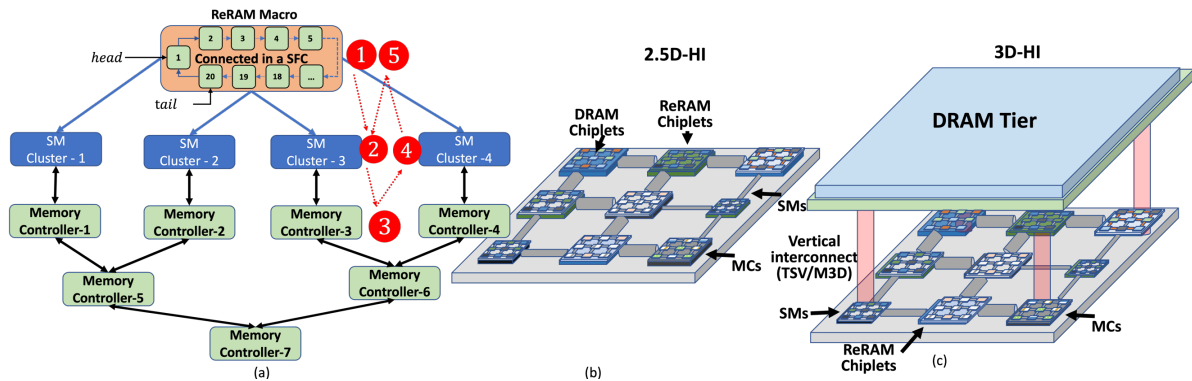


Fig. 2: Overview of the (a) proposed heterogeneous architecture dataflow. ❶-❺ describe the dataflow within each computation kernel; (b) 2.5D heterogeneous integration; (c) 3D heterogeneous integration for accelerating Transformer model.

Multiple attention heads are processed in parallel, and the resultant matrices are concatenated and multiplied with the weight matrix W_i^O , which maps the attention probabilities to output scores before advancing the output to the FF layers where N is the input-sequence length (given by (7)).

$$H^{MHA} = \text{concat}(P_i W_i^O) \forall i \in N \quad (7)$$

Once the score is computed within the multi-head self-attention block, we add the input to the output of the multi-head attention and normalize the resultant matrix. This step is the layer-norm operation employed to reduce covariance shifts within the fully connected (FC) layer [20]. GeLU is the commonly used activation function in Transformers [2] [24] [25]. For modern large language models (LLMs), FC layers dominate the runtime of the decoder block since the model dimension d_{model} is much larger than the input sequence length N and the context length $l_{context}$, thus $O(Nd_{model}^2) \gg O(l_{context}^2 d_{model})$. For example, more than 99% of MVM operations in GPT-3 are spent on executing the FC layers. Since the FC layers are not frequently updated, they are static and have significant weight overlap in each encoder-decoder stack. Therefore, we utilize ReRAM chiplets for the FF [14].

To summarize, we use a combination of SM-MC-DRAM and ReRAM chiplets placed on a 2.5D interposer to execute the end-to-end Transformer models. Due to this heterogeneity, analyzing the inter-chiplet traffic patterns is imperative to design the overall NoI architecture.

3.2 Communication between Computation Kernels

Fig. 2(a) shows the overall dataflow in the heterogeneous chiplet platform. Various components of the NoI traffic are:

Input Embedding: The input embedding provides each token with an input representation. The tokenization is a series of MVM on the input sequence where the overall computation is sequentially distributed among multiple ReRAM chiplets. Data always flows from the i^{th} to the $(i + 1)^{th}$ chiplet. Hence, contiguity should be maintained on the physical NoI layer, to the extent possible, between any two consecutive chiplets to reduce the communication overhead. Since existing NoI architectures are primarily based on standard multi-hop regular topologies such as a mesh or a torus, it may not always be possible to find contiguously placed chiplets available to map successive parts of the input embedding. If two consecutive layers are mapped far apart, it will lead to long-range multi-hop communication through the NoI. This, in turn, will degrade the performance and energy efficiency of the NoI and hence the overall system. Therefore, we connect the ReRAM chiplets using space-filling curves (SFCs). This dataflow-awareness within computational kernels has been previously exploited

for designing a NoI called Floret for large-scale CNN inferencing using SFC [25]. SFCs are a specialized class of algorithmic mapping techniques that have found significant application in locality-preserving data structure for numerous scientific applications that involve spatial and range queries [26]. More specifically, an SFC maps a multi-dimensional point cloud onto a single dimension; therefore, each SFC represents a linear ordering of the input set of points. Numerous types of SFCs have been defined over the decades, including simple schemes such as row/column major curves to more sophisticated curves such as the Hilbert curve [28], Morton or Z-curve [30], or onion curve [31]. For a review of classical SFCs, please refer to [32,33].

This operation is referenced as ❶ in the Fig. 2(a). Our approach connects the ReRAM chiplets (in the order of data flow) along the contiguous path formed by the SFC. The SFC stitches multiple chiplets contiguously and has a head and a tail that connect the chiplets linearly (Fig. 2 (a)).

KQV Computation: We implement this step, which is the starting part of the self-attention mechanism using SM, MC, and DRAM chiplets. After computing each input token generated in Step 1, W_k, W_Q, W_V need to be loaded. We use the FlashAttention dataflow to partition the matrices onto the SMs [27]. This operation can be effectively performed using DRAM (HBM2) with multiple SM chiplets for each MC partition. The data transmission happens in two steps. First, for each head h , W_k, W_Q, W_V are loaded in the SMs through the MCs. Then, the corresponding K, Q, V is computed for each input token. This gives rise to SM to MC data exchange. Due to many SMs and a limited number of MCs, this results in a many-to-few data flow. These steps are shown as ❷ & ❸ in Fig. 2(a). The placement of the DRAM chiplet also contributes to the overall latency. We consider two types of DRAM placements. In the first configuration, SM, MC, and DRAM are all distributed over the 2.5D interposer. We call it 2.5D heterogeneous integration (2.5D-HI), shown in Fig. 2(b). In the second configuration, the DRAM is vertically mounted over the MC clusters. This is called 3D heterogeneous integration (3D-HI), shown in Fig. 2(c). We will consider both of these configurations in our performance evaluation.

Score Computation: This is the final step of the self-attention to multiply the attention score matrix S after Softmax by the V matrix before the FF layer (shown as ❹ in Fig. 2(a)). The placement of SM and MC chiplets is critical for the latency and energy consumption.

Feed Forward Layer: The FF network consists of two consecutive FC layers, which are large static hidden layers. Like DNN models, the fully connected layers have fixed sizes and sparse weight updates compared to encoder outputs. The FC layers have dataflow from layer L_i to layer L_{i+1} connection. The activations and corresponding weights of the adjacent layers must be mapped in a contiguous manner. Hence, there is a need to maintain contiguity on the physical NoI layer, to the extent possible, between the neural layers to reduce communication overhead. This is identical to the dataflow pattern observed in the case of Input Embedding generation. Hence, like ❶, an SFC is employed to maintain contiguity among communicating layers mapped on the ReRAM chiplets. The ReRAM macro refers to a set of ReRAM chiplets employed to execute computations in the feed-forward layers contiguously, thereby reducing communication overhead within a Network on Interconnect (NoI). This part of the execution is shown as ❺ in Fig. 2(a). We repeat the above-described dataflow loop starting from ❷ for the next encoder as Input Embedding is a one-time process in the overall execution flow. It should be noted that the same ReRAM macro is used for ❶ and ❺ as they execute on different time stamps. This macro of ReRAM chiplets maintains data flow between consecutive layers efficiently, leveraging SFCs to preserve locality

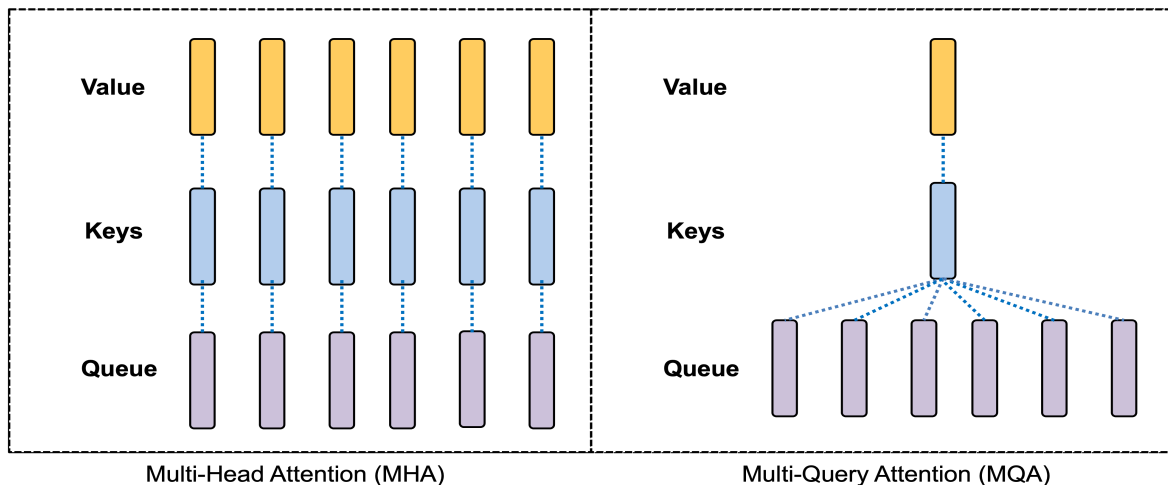


Fig. 3: High-level illustration of the difference between multi-head attention (MHA) and multi-query attention (MQA).

and enhance the performance and energy efficiency of the overall system. Hence, we consider all the ReRAM chiplets together as a *ReRAM macro*. In the NoI design, we optimize the location of the ReRAM macro with respect to SM, MC, and DRAM chiplets.

The original transformer model with encoder-decoder blocks is designed for translation-class of natural-language processing (NLP) tasks [28]. However, the transformer architectures evolve continuously with structural variations tailored to other NLP tasks. Several transformer architectures have recently been proposed, including transformers composed of decoder-only (GPT-class of transformer models) or encoder-only (BERT-class of transformer models) blocks. This effectively divides the model complexity in half, reducing the computational requirements.

Additionally, numerous architectural refinements have also emerged within the encoder/decoder block. One such advancement is the introduction of Multi-Query Attention (MQA). MQA is specifically designed to enhance the efficiency of attention mechanisms [29] [30]. MQA, unlike the standard multi-head attention (MHA), utilizes the same K and V values across heads while assigning distinct Q vectors to each head. Fig. 3 shows the difference between MHA and MQA. MQA shares a single key and value head across all query heads. The amount of computation performed by MQA is equivalent to the standard MHA. However, the key difference is the reduced amount of data exchange from memory to chiplets.

Another variation is the parallel attention framework, which executes the model with both the attention and FF layers operating concurrently [30]. The model modifies the computational kernel in each transformer block and employs a parallel formulation as opposed to the conventional “serialized” formulation. The standard formulation, in this context, can be expressed as:

$$Y = x + MLP\left(LayerNorm\left(x + Attention(LayerNorm(x))\right)\right) \quad (8)$$

In contrast, the parallel formulation can be described as:

$$Y = x + MLP(LayerNorm(x)) + Attention(LayerNorm(x)) \quad (9)$$

The parallel formulation (given in (9)) facilitates a pipelined execution of attention and feed-forward computations, thereby achieving higher speedup. We consider all these variations (encoder/decoder-only, MQA, and parallel attention) and propose a model-agnostic NOI tailored for different classes of transformer models.

3.3 NoI Design Optimization

Considering the traffic patterns mentioned above, we need to place the DRAM, the ReRAM Macro, SM, and MC chiplets on the interposer to maximize throughput and minimize the data exchange latency to accelerate the Transformer model inferencing. Suppose each candidate design (λ) in the NoI design space corresponds to a specific placement of the chiplets along with the routers and inter-router links. Our goal is to achieve high throughput under the given application traffic pattern. Minimizing the mean $\mu(\lambda)$ and standard deviation $\sigma(\lambda)$ of the traffic distribution leads to an overall higher throughput of the candidate NoI designs.

MOO Formulation: The design of heterogeneous NoI architecture can be formulated as a multi-objective optimization (MOO) problem. We can represent the MOO formulations as follows:

$$\lambda^* = MOO(\text{objective} = \mu(\lambda), \sigma(\lambda)) \quad (10)$$

where λ^* is the set of Pareto optimal designs. Here, we aim to find the optimal placement of chiplets and associated routers and links such that the design requirements for all the elements are satisfied. Each candidate NoI design must be evaluated efficiently to help guide our search for the best NoI architecture. Below, we describe the critical elements of our MOO formulation.

- 1) **Design Variables:** There are two types of design variables for NoI-based chiplet design $\lambda = (\lambda_c, \lambda_l)$, where λ_c corresponds to a candidate placement of chiplets and λ_l corresponds to a candidate placement of communication links between chiplets.
- 2) **Constraints:** We have two constraints to define a feasible solution space. First, the NoI should enable data transfer between any two pair of chiplets, i.e., it should connect all chiplets with no islands. Second, the number of links used to design NoI should not exceed that in a 2-D mesh. However, with an efficient NoI, we can reduce the number of links compared to a mesh NoI [9].

Objectives: Our objective is to maximize the system throughput. Specifically, we consider optimizing two objectives, namely, the mean $\mu(\lambda)$ and standard deviation $\sigma(\lambda)$ of the traffic utilization u_k on each communication link k at time t , determined by the NoI frequency. Note that the F_{ij} , the amount of traffic between chiplets i and j , respectively, can be obtained by profiling the application workload, i.e., inference of Transformer models.

These parameters are defined as follows:

$$u_k = \sum_{i=1}^L \sum_{j=1}^L F_{ij}(t) \cdot q_{ijk} \quad (11)$$

$$\mu(\lambda, t) = \frac{1}{P} \times \sum_{k=1}^P u_k \quad (12)$$

$$\sigma(\lambda, t) = \sqrt{\frac{1}{P} \sum_{k=1}^P (u_k - \mu(\lambda, t))^2} \quad (13)$$

where L represents the number of routers and P represents the number of links in the system, as mentioned earlier, q_{ij} is a Boolean representation if link k is being used between router i and router j .

$$q_{ijk} = \begin{cases} 1, & \text{if chiplet } i, j \text{ communicate across link } k. \\ 0, & \text{otherwise} \end{cases}$$

To compute the average throughput across all timestamps, we take a time average of the mean $\mu(\lambda)$ and standard deviation $\sigma(\lambda)$ as represented in (14) and (15):

$$\mu(\lambda) = \text{avg } \mu(\lambda, t) \quad (14)$$

$$\sigma(\lambda) = \text{avg } \sigma(\lambda, t) \quad (15)$$

Once we solve the MOO problem to obtain the Pareto optimal NoI designs λ^* among all possible system configurations, we perform cycle-accurate simulations for each design in λ^* to find the design with the lowest EDP and lower latency than a mesh NoI simultaneously.

MOO Solver: Prior work has shown that we can significantly improve the accuracy and speed of design optimization by utilizing knowledge gained from the past explored designs. The key idea is to extract relevant knowledge from previously explored designs to intelligently guide the search to more promising parts of the design space. In this work, we adopt the MOO-STAGE, a MOO algorithm that belongs to this class of data-driven methods, for the problem of NoI design, noting that any other MOO solver can be used. The key idea behind MOO-STAGE is to learn an evaluation function to select good starting states to guide local search procedures such as greedy search toward better local optima. MOO-STAGE is an iterative algorithm which has been shown to converge faster in comparison to AMOSA or regression-based optimization [31]. Each iteration consists of the following three steps. First, we use the current evaluation function to select a good starting state for the local search procedure. Second, we perform a local search from this selected starting state until we reach a local optimum and compute the quality of the corresponding Pareto set in terms of Pareto-hyper volume (PHV) as a metric [9] [31]. Third, we update the evaluation function based on the training data from the local search runs. As the evaluation function improves with the training data over iterations, it effectively prunes the design space and directs the search toward more promising regions. If the evaluation function is accurate, it will avoid bad starting states and select promising starting designs to improve the efficiency and accuracy of design optimization. Otherwise, we update the evaluation function to minimize errors. To update the evaluation function, we use random forest, which was shown to be a fast and accurate learner, to create effective evaluation functions [9] [31]. Ultimately, our target is to find an optimized NoI design with fewer links. More details and convergence comparisons to other state-of-the-art MOO strategies can be found in existing literature [31]. Once we solve the MOO problem to obtain the Pareto optimal NoI designs with suitable chiplet, link, and router configurations and placements, we perform cycle-accurate simulations to determine the overall performance and select the best NoI.

4 EXPERIMENTAL RESULTS

In this section, we first introduce the experimental setup to evaluate the performance of the proposed HI architecture. Next, we describe the transformer model considered in our evaluation. Subsequently, we present a thorough performance evaluation of the 2.5D-HI and 3D-HI architecture. Finally, we present a comparative performance evaluation of the proposed architecture with respect to state-of-the-art baselines.

4.1 Experimental Setup:

4.1.1 System Specification and Evaluation Setup:

Our performance evaluation considers three system sizes of 36, 64, and 100 chiplets. Within each system configuration, we maintain a SM-MC ratio of 8:1, consistent with the Volta architecture [32] [33]. Each MC is connected to a DRAM chiplet. The ReRAM chiplets are allocated based on the dimensions of the FF network. To illustrate, in the case of a 100

chiplet system, we divide the 3D-HI system into 64 SMs, 8 MCs along with 8 DRAM chiplets corresponding to 8 partitions of the HBM2 memory, and 20 ReRAM chiplets connected as a ReRAM macro. Note that this is an example system size, and the proposed design methodology and evaluation scheme are valid for other system configurations.

SMs are based on the NVIDIA Volta architecture with 10 Tensor cores along with the scratchpad memory for arithmetic operations. The group of collocated SMs (SM cluster in Fig. 2 (a)) are associated with a particular MC. Following prior work, we consider each ReRAM chiplet to consist of 16 ReRAM tiles and peripheral circuits such as accumulator, buffer, activation, and pooling units [7]. Each tile consists of multiple processing elements (PEs) comprising 128×128 ReRAM crossbar arrays. Each tile has 96 PEs connected with an H-Tree-based point-to-point network [7] [34].

We obtain the workload traces using Nvidia-smi with Nvidia A40 GPU to evaluate the performance and energy efficiency of the system. The software stack for running the Transformer model to obtain the traffic pattern is built on top of the CuDNN 12.2 with PyTorch, consistent with prior work [17]. For ReRAM chiplets, we use a modified NeuroSim to implement the MVM operations involved in the Input Embedding and the FF layers in the Transformer model [5]. Further, we use the cycle-accurate BookSim2 simulator to implement the interconnection network to connect the chiplets via different NoI architectures [5] [7]. The inputs to the BookSim2 are the connectivity between NoI routers and the inter-chiplet traffic traces for the Transformer model. The simulator outputs area, latency, and NoI energy consumption. Considering the clock frequency of 1.2GHz, each 1.55 mm link can be traversed in one cycle. The longer links are divided into multiple stages, where each stage is 1.55 mm long. All the vertical links (in the case of 3D-HI) are traversed in one cycle. We employ the Nvidia ground-referenced signaling (GRS) parameters for an interconnection network designed using 32nm technology to evaluate the NoI area and power consumption [5].

We compare the performance and energy efficiency of the HI architectures (2.5D-HI and 3D-HI) with the recently proposed state-of-the-art HAIMA and TransPIM architectures on various sequence lengths [2] [3]. Though Xformer and HAIMA have very similar architecture, we consider HAIMA in this performance evaluation as it has been shown to outperform Xformer. We redesigned HAIMA and TransPIM on the chiplet-based system as HAIMA_chiplet and TransPIM_chiplet, respectively. In both HAIMA_chiplet and TransPIM_chiplet, we implement the same MOO algorithm as the proposed HI configurations to suitably place the chiplets, routers, and associated links to give a fair optimization as we follow in comparative heterogeneous architectures. We maintain an iso-chiplet configuration across all architectures and system sizes, where the physical area of each chiplet is $10mm^2$.

4.1.2 Datasets and Transformer Workloads

We consider six transformer models in our experimental evaluation: BERT-Base, BERT-Large, BART-Large, Llama2-7B, and GPT-J [30] [29] [28]. These models represent diverse transformer architectures, including Encoder-Decoder,

Table 1: Transformer Model and Parameters

Model	Transformer Architecture	d_{model}	Layers	Heads	Parameters (In millions)
BERT-Base	Encoder Only	768	12	12	110
BERT-Large	Encoder Only	1024	24	16	340
BART-Base	Encoder-Decoder	768	12	12	140
BART-Large	Encoder-Decoder	1024	12	16	400
GPT-J	Decoder Only	4096	28	16	6700
Llama2-7B	Decoder Only	4096	32	32	7000

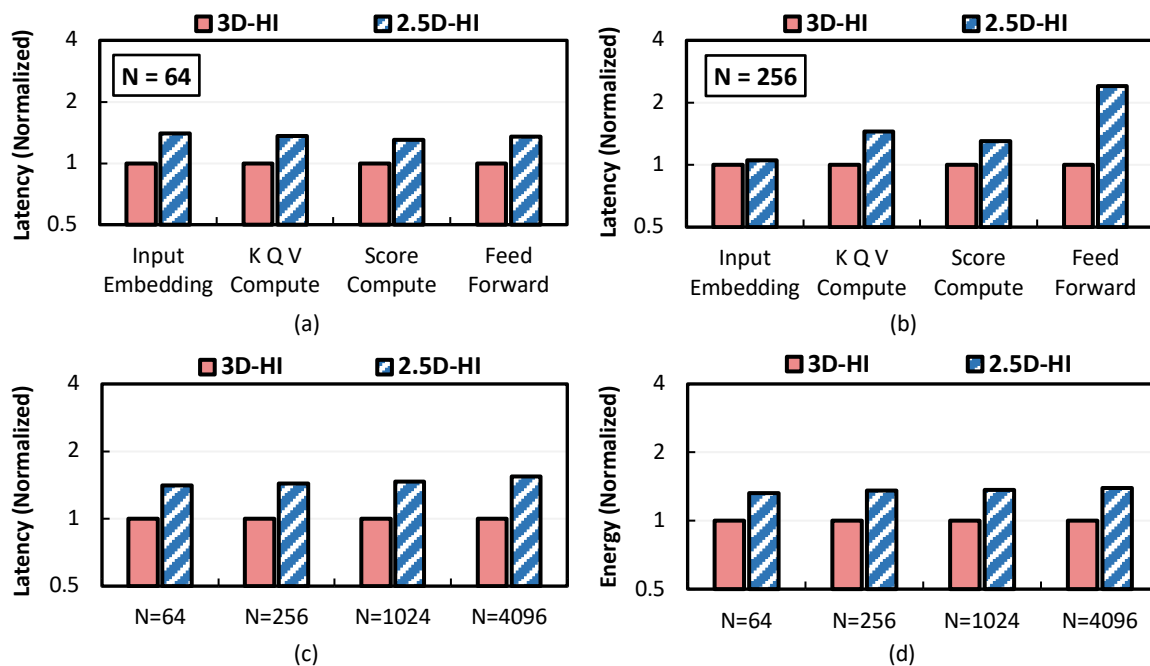


Fig. 4: Latency improvement for each computational kernel of the NoI architecture comparing 3D-HI vs 2.5D-HI for (a) $N=64$ & (b) $N=256$; (c) End-to-end latency; and (d) energy improvement of 3D-HI vs 2.5DHI.

Encoder/Decoder only, MQA, and parallel MHA-FF architectures. BERT adopts an encoder-only transformer architecture, while BART incorporates both encoder and decoder blocks. Llama2-7B and GPT-J are decoder-only models. Llama2-7B uses MQA instead of MHA for attention computation, whereas GPT-J employs Parallel MHA-FF computation. Table I presents the different Transformer models considered in our experimental evaluation and their details, including model dimensions, number of heads, number of layers, and number of parameters.

First, we evaluate a 36-chiplet system with BERT-Base. As the system size increases, we progressively employ models with increased parameter counts to illustrate the scalability of the proposed HI architecture. Specifically, we extend our evaluation to a 64-chiplet system with BERT-Large and BART-Large. Finally, we scale up to a 100-chiplet system with Llama2-7Bs and GPT-J, where the number of parameters approaches billions.

4.2 Effect of Heterogenous Integration on Performance

This sub-section compares performance evaluation between the two HI architectures (2.5D-HI vs. 3D-HI). Figs. 4 (a) & (b) show the latency profile of each computational kernel for a relatively short ($N=64$) and long ($N=256$) sequence, respectively. The 3D-HI architecture outperforms the 2.5D-HI counterpart for all the computational kernels. The performance gain depends on both the sequence length and the kernel characteristics. The primary reason behind 3D-HI's performance gain is the more degree of freedom in chiplet placement enabled by the vertical integration (connecting MC to DRAM vertically). Fig. 5 shows the hop count distribution on 2.5D-HI and 3D-HI for the sequence length of 256 as an example. We observe that 3-hop paths are the most frequent in the case of the 2.5D-HI architecture with considerable 5- and 6-hop paths. In the case of 3D-HI, the peak moves towards the left with the mean hop count of 1.5. For 2.5D-HI, DRAM and ReRAM chiplets are constrained to be placed on the same plane due to the limited floorplan options.

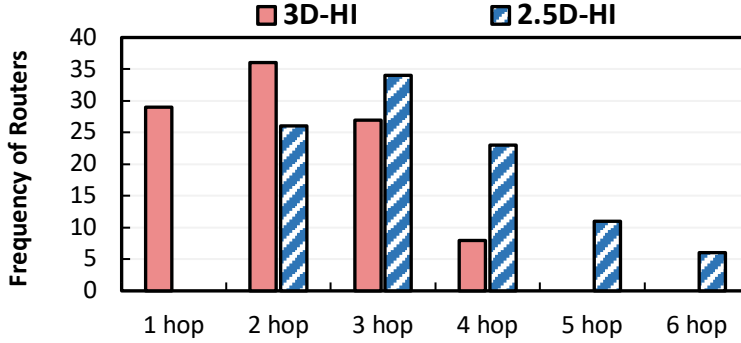


Fig. 5: Average Hop count comparing 3D-HI & 2.5D-HI. The peak in the case of 3D-HI is moving towards the left.

Conversely, the vertical layer in 3D-HI provides an additional degree of freedom for placing the DRAM chiplets. This, in turn, facilitates lower average hop count in 3D-HI.

It is also interesting to see that the performance gain of 3D-HI over 2.5D-HI diminishes for longer sequence length for Input embedding. For longer sequence lengths, the input embedding computation on ReRAM chiplets is bottlenecked by the DRAM-MC loading, which cannot be alleviated by using 3D-HI. However, as the ReRAM computation on the FF layer depends only on the fixed-size kernels, it does not depend on the DRAM-MC access. Hence, the performance benefit of faster MVM operation on ReRAM chiplets is predominant in FF for all the sequence lengths. 3D-HI consistently outperforms 2.5D-HI in (K, Q, V) and score computation due to faster DRAM access. For brevity, we show the individual kernel performance gain with two sequence lengths ($N = 64$; $N = 256$). However, we observe the same trend for all other sequence lengths. Figs. 4 (c) & (d) show the end-to-end latency and energy consumption profiles of 2.5D-HI and 3D-HI configurations for different sequence lengths. 3D-HI outperforms 2.5D-HI for all sequence lengths. Hence, we use 3D-HI in the following comparative performance evaluation with the current state-of-the-art chiplet based accelerators.

4.3 Full System Evaluation

Next, we undertake a full system performance evaluation and compare the overall execution time and energy consumption of 3D-HI with respect to the TransPIM_chiplet and HAIMA_chiplet for multiple sequence lengths. Following prior work, TransPIM_chiplet consists of multiple auxiliary compute units (ACUs) to enable computing near DRAM chiplets. ACUs perform vector reduction and Softmax function [2]. Other computational kernels are calculated with a bit-serial row-parallel scheme. The token sharding technique is employed as the optimal dataflow strategy. This enables DRAM chiplets to compute the partial attention score matrix independently without communicating with other chiplets. In the case of HAIMA_chiplet, SRAM chiplets compute specific parts of the score computation (equation (5) & (6)). DRAM chiplets are employed for implementing self-attention and FF layers. Following the original HAIMA framework, we use multiple host chiplets to compute the arithmetic operations [3].

Figs. 6(a) & (b) show the latency profiles for different computational kernels for 3D-HI, TransPIM_chiplet, and HAIMA_chiplet for two sequence lengths (64 and 256) as examples. We observe that 3D-HI has lower latency than both TransPIM_chiplet and HAIMA_chiplet for all the computing kernels. For self-attention (K, Q, V, and Score computation), we see consistent performance gains over TransPIM_chiplet and HAIMA_chiplet. The tensor cores of the SMs in 3D-HI enable the performance gain for self-attention. However, the performance gain is maximum for the FF layer due to the efficient computation by ReRAM chiplets. The SMs efficiently accelerate MHA computation, and the ReRAM layer computes the FF layer in parallel. In contrast, both HAIMA and TransPIM have latency overhead in a chiplet-architecture.

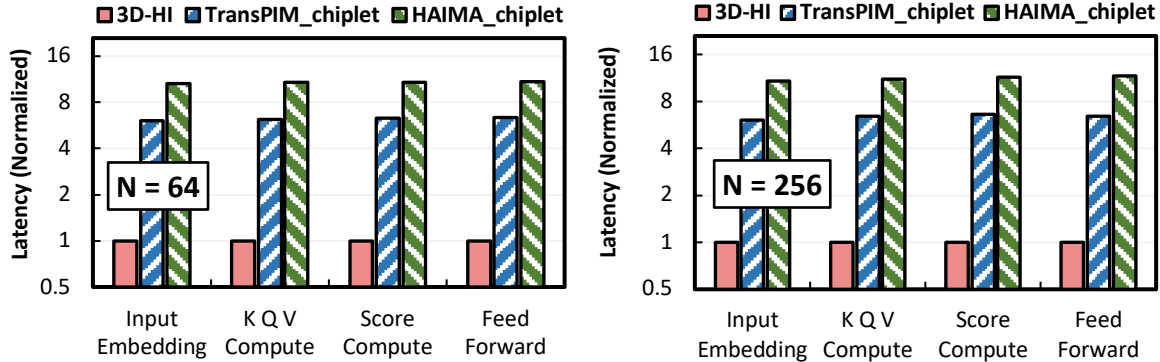


Fig. 6: Latency improvement for each computational kernel of the NoI architecture comparing 3D-HI with counterparts for $N=64$ & $N=256$ for 36 chiplet system.

HAIMA maximizes the throughput by activating multiple banks within the DRAM-PIM parallelly. In 2.5D systems, these banks need to be disintegrated into chiplets, which leads to higher power consumption and frequent data exchange between SRAM and DRAM chiplets and gives rise to multiple contention paths. This leads to higher latency overheads and reduced energy efficiency compared to 3D-HI and a simpler ring broadcast-based communication dataflow proposed in TransPIM. Additionally, 3D-HI benefits from the fused score and Softmax calculations on the SM chiplets. However, HAIMA and TransPIM use additional host access, which prevents online execution as it results in repeated data exchange with the host and hence incurs additional communication latency. Although HAIMA outperforms TransPIM in score computation, TransPIM has faster execution and lower energy consumption since it performs the FF network more efficiently. It should be noted that the implementation of SFC-based NoI for the feed-forward layers in TransPIM_chiplet and HAIMA_chiplet is not feasible due to non-deterministic traffic and continuous memory access dependencies, preventing the isolation of a dedicated sub-system exclusively for the FF layer. With HI, this constraint is mitigated by having a dedicated computational platform (ReRAM chiplets) to enable FF network processing.

We do not consider the ReRAM-only architecture, ReTransformer in this comparative performance evaluation for two reasons [1]. First, the ReTransformer architecture only focuses on speeding up self-attention with no full system evaluation. Second, the ReRAM-only architecture has endurance and reliability issues when accelerating Transformer models. For example, consider the BERT model with $h = 8$ heads and sequence length $n = 4096$. In this case, for the ReRAM chiplet, each with 16 tiles with 40 crossbar arrays of 128×128 storing 2 bits, we have 5KB of storage for a single write. In the case of self-attention specifically, W_K, W_Q, W_V (512×64 matrices with each element represented in a 16-bit precision) and the K, Q, V computation generates about 10^7 writes ($\sim 30\text{Gb}$) per ReRAM cell per token. For longer sequence lengths such as $N=4096$, the rewrites increase to 10^{10} in a single encoder. In the case of subsequent $Score, P_i$, and H^{MHA} , writes are of the order 10^7 . As the models grow following previous trends (GPT4, Llama2-70B with 170B parameters), the write updates would invoke serious endurance and reliability challenges for a ReRAM-only architecture [25]. 3D-HI avoids this challenge by integrating heterogenous chiplets on the 2.5D interposer and accelerating only the static parts (i.e., no write updates) of the computation using ReRAM chiplets. Hence, a heterogenous integration approach is imperative for accelerating Transformer models.

4.4 System Scalability of the Heterogenous Architecture

We extend our framework to larger models on 64 and 100 chiplet systems to demonstrate system scalability. Figs. 7(a) & (b) presents a comparative analysis showing full system (end-to-end) latency and energy for 3D-HI, TransPIM_chiplet,

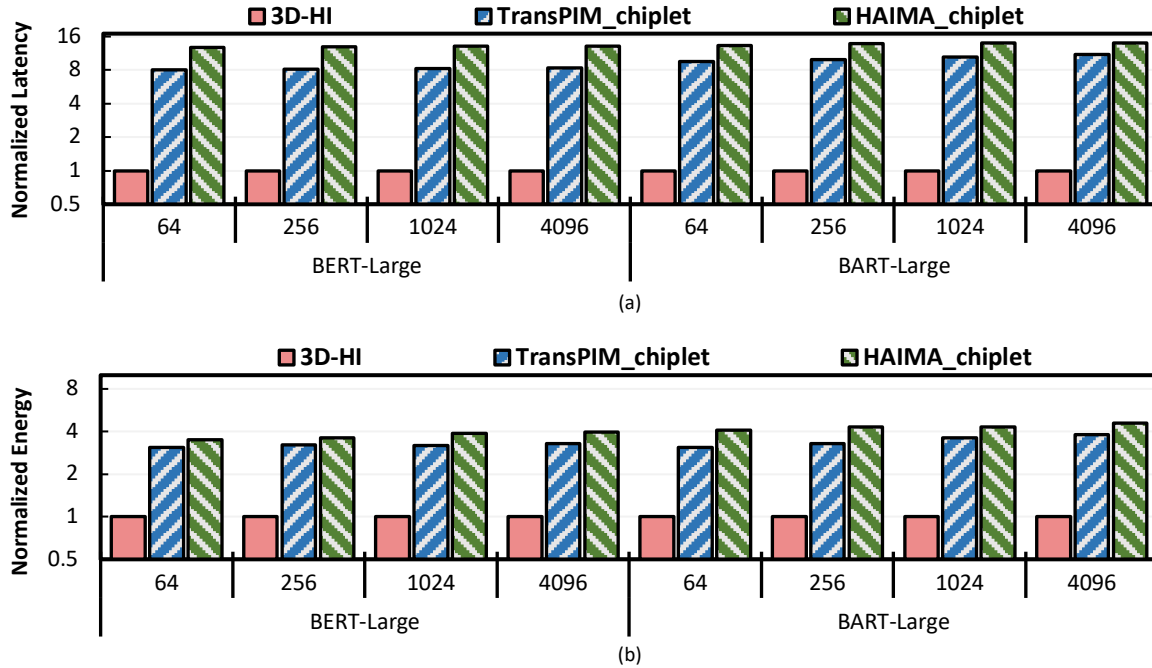


Fig. 7: End-to-end energy improvement of the 3D-HI over its counterparts for 64 chiplet system running BERT-Large and BART-Large and HAIMA_chiplet running BERT-Large and BART-Large on a 64-chiplet system. We observe that 3D-HI consistently outperforms both TransPIM_chiplet and HAIMA_chiplet in terms of latency as well as energy consumption for all considered sequence lengths. Notably, the performance gain for 3D-HI increases with the input sequence length, showing scalability over sequence length. For instance, the latency gain increases from 13.3x to 14.1x as the input sequence length increases from 64 to 4096 for BERT-Large. Similarly, energy gain for 3D-HI also increases as the sequence length increases with respect to HAIMA_chiplet and TransPIM chiplet. This performance enhancement is primarily due to 3D-HI, which ensures each computational kernel of the Transformer model is executed on the appropriate hardware platform. Further, long-range communication is minimized on the 3D-HI system. Unlike HAIMA_chiplet and TransPIM_chiplet, the softmax computation is performed online on the SM cores without necessitating any computation on the host device leading to communication bottlenecks. Further, during the execution of the feed-forward layer, the entire data flow is confined within the ReRAM macro, interconnected as a SFC. This minimizes contention issues due to limited data access outside of the ReRAM macro to other chiplets.

Next, we extend our system to 100 chiplet configurations and evaluate bigger transformer models featuring billions of parameters. Figs. 8(a) & (b) show the end-to-end latency and energy for Llama2 and GPT-J on the 100 chiplet system. We observe increased speedup in comparison to the 64 chiplet configuration. Specifically, we note up to 22.8x gain in latency and 5.36x lower energy consumption with respect to the baselines. 3D-HI architecture demonstrates scalability, exhibiting faster execution as the transformer model size and input sequence length increase. In contrast, HAIMA_chiplet and TransPIM_chiplet confront scalability challenges when accommodating larger model sizes. This is attributed to the increased communication overhead for TransPIM and HAIMA chiplets, with the number of hops increasing as the system grows due to long-range communication. These observations underscore the effectiveness of 3D-HI architecture and the NOI design in addressing the demands of larger-scale Transformer models, exhibiting superior scalability and performance.

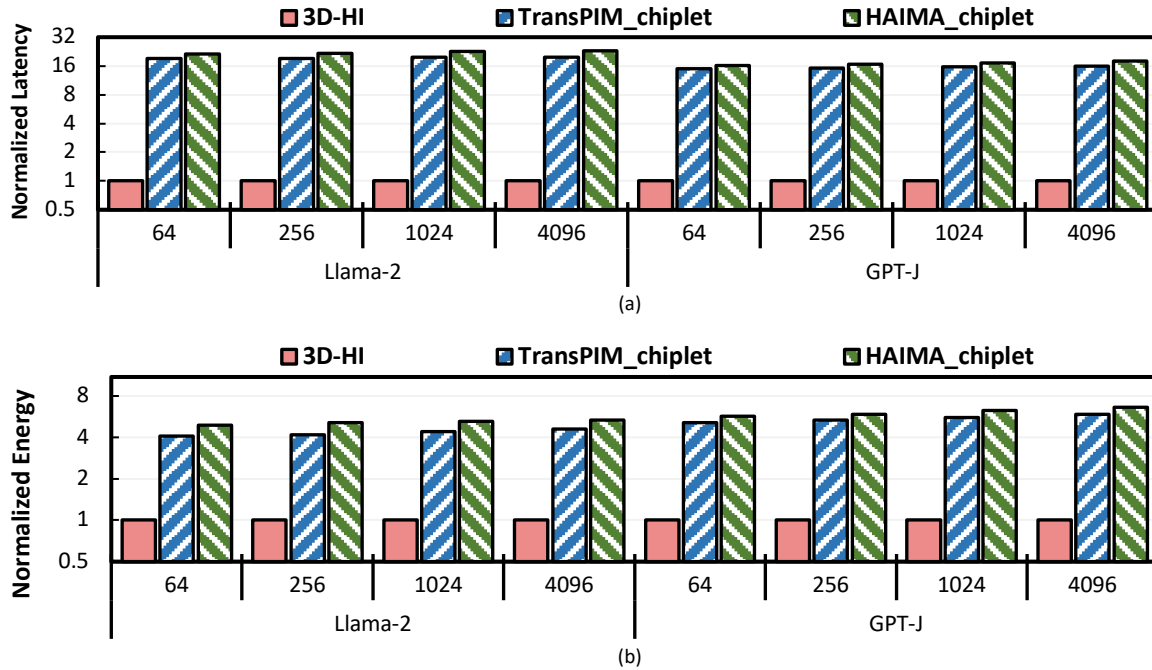


Fig. 8: End-to-end energy improvement of the 3D-HI over its counterparts for 100 chiplet system running Llama2-7B and GPT-J

5 CONCLUSION

The end-to-end transformer model exhibits significant heterogeneity in its computational kernels, necessitating the integration of different types of hardware modules on a single system for high-performance and energy-efficient acceleration. This paper considers different heterogeneous chiplets to design a multi-chiplet architecture called 3D-HI for accelerating Transformer models. 3D-HI uses SM-MC cores for multi-head attention and ReRAM cores for the feed-forward network, which optimize both achievable energy efficiency and throughput. The heart of the 3D-HI platform is a NoI architecture that enables efficient computing kernel to chiplet mapping for the complex interactions among heterogeneous chiplets. Further, vertical integration on top of a 2.5D interposer helps to enhance overall system performance and alleviates the issue of memory bottlenecks. Experimental results demonstrate that 3D-HI lowers the latency and energy consumption by up to $22.8\times$ and $5.36\times$ with respect to an equivalent state-of-the-art chiplet-based platform. Notably, 3D-HI exhibits versatility across various transformer models/sizes and shows consistent speedup irrespective of the model.

REFERENCES

- [1] X. Yang, B. Yan, H. Li and Y. Chen, "ReTransformer: ReRAM-based Processing-in-Memory Architecture for Transformer Acceleration," in *ICCAD*, San Diego, 2020.
- [2] M. Zhou, W. Xu, J. Kang and T. Rosing, "TransPIM: A Memory-based Acceleration via Software-Hardware Co-Design for Transformer," in *HPCA*, Korea, 2022.

- [3] Y. Ding et al., "HAIMA: A Hybrid SRAM and DRAM Accelerator-in-Memory Architecture for Transformer," in *DAC*, 2023.
- [4] A. Kannan, N. Jerger and G. Loh, "Enabling interposer-based disintegration of multi-core processors," in *MICRO*, 2015.
- [5] G. Krishnan et al., "SIAM: Chiplet-based Scalable In-Memory Acceleration with Mesh for Deep Neural Networks," *ACM Trans. Embed. Comput. Syst*, vol. 20, no. 5, pp. 1-24, 2021.
- [6] S. Bharadwaj, J. Yin, B. Beckmann and T. Krishna, "Kite: A Family of Heterogeneous Interposer Topologies Enabled via Accurate Interconnect Modeling," in *DAC*, 2020.
- [7] P. Vivet et al., "IntAct: A 96-Core Processor With Six Chiplets 3D-Stacked on an Active Interposer With Distributed Interconnects and Integrated Power Management," *IEEE Journal of Solid-State Circuits*, vol. 56, no. 1, 2021.
- [8] H. Sharma et al., "Achieving Datacenter-scale Performance through Chiplet-based Manycore Architectures," in *DATE*, 2023.
- [9] H. Sharma et al., "SWAP: A Server-Scale Communication-Aware Chiplet-Based Manycore PIM Accelerator," *IEEE Transactions on Computer-Aided Design of Integrated Circuits and Systems*, vol. 41, no. 11, pp. 4145-4156, 2022.
- [10] Y. Shao et al., "Simba: Scaling Deep-Learning Inference with Multi-Chip-Module-Based Architecture," in *MICRO*, 2019.
- [11] Z. Tan, H. Cai, R. Dong and K. Ma, "NN-Baton: DNN Workload Orchestration and Chiplet Granularity Exploration for Multichip Accelerators," in *ISCA*, 2021.
- [12] A. Graening, S. Pal and P. Gupta, "Chiplets: How Small is too Small?," in *DAC*, 2023.
- [13] P. Iff et al., "HexaMesh: Scaling to Hundreds of Chiplets with an Optimized Chiplet Arrangement," in *DAC*, 2023.
- [14] S. Sridharan, J. Stevens, K. Roy and A. Raghunathan, "X-Former: In-Memory Acceleration of Transformers," in *arXiv:2303.07470*, 2023.
- [15] H. Wang, Z. Zhang and S. Han, "Spatten: Efficient sparse attention architecture with cascade token and head pruning," in *ArXiv*, vol. *abs/2012.09852*, , 2020.
- [16] T. J. Ham et al., "A3: Accelerating attention mechanisms in neural networks with approximation," in *HPCA*, 2020.
- [17] M. He et al., "Newton: A dram- maker's accelerator-in-memory (aim) architecture for machine learning," in *MICRO*, 2020.
- [18] T. Tambe et al., "EdgeBERT: Sentence-Level Energy Optimizations for Latency-Aware Multi-Task NLP Inference," in *MICRO*, 2021.
- [19] S. Tuli and N. K. Jha, "AccelTran: A Sparsity-Aware Accelerator for Dynamic Inference with Transformers," in *arXiv:2302.14705*, 2023.
- [20] S. Tuli and N. K. Jha, "TransCODE: Co-design of Transformers and Accelerators for Efficient Training and Inference," in *arXiv:2303.14882*, 2023.
- [21] C. Kwon et al., "25.4 A 20nm 6GB Function-In-Memory DRAM, Based on HBM2 with a 1.2TFLOPS Programmable Computing Unit Using Bank-Level Parallelism, for Machine Learning Applications," in *ISSCC*, 2021.
- [22] J. Fang, Y. Yu and C. Z. J. Zhao, "TurboTransformers: An Efficient GPU Serving System For Transformer Models," in *DPCC*, 2021.
- [23] S. Resch et al., "On Endurance of Processing in (Nonvolatile) Memory," in *ISCA*, 2023.

- [24] S. Pati et al., "Demystifying BERT: implications for accelerator design," in *arXiv preprint arXiv:2104.08335*, 2021.
- [25] H. Sharma et al., "Florets for Chiplets: Data Flow-aware High-Performance and Energy-efficient Network-on-Interposer for CNN Inference Tasks," *ACM Transactions on Embedded Computing Systems*, vol. 22, no. 5, pp. 1-21, 2023.
- [26] M. Haque, A. Kalyanaraman, A. Dhingra, N. Abu-Lail and K. Graybeal, "DNAjig: a new approach for building DNA nanostructures.," in *International Conference on Bioinformatics and Biomedicine*, 2009.
- [27] T. Dao, D. Y. Fu, S. R. A. Ermon and C. Ré, "FlashAttention: Fast and Memory-Efficient Exact Attention with IO-Awareness," in *arXiv:2205.14135*, 2022.
- [28] D. Jacob et al., "Bert: Pre-training of deep bidirectional transformers for language understanding.," *arXiv:1810.04805*, 2018.
- [29] "Alpaca Foundation Model with 7B Parameters.," Stanford, [Online]. Available: https://github.com/tatsu-lab/stanford_alpaca#data-release. [Accessed 22 Nov 2023].
- [30] "LLaMA Collection of Foundation Models.," Meta, [Online]. Available: <https://github.com/facebookresearch/llama>. [Accessed 22 Nov 2023].
- [31] B. Joardar et al., "Learning-Based Application-Agnostic 3D NoC Design for Heterogeneous Manycore Systems," *IEEE Transactions on Computers*, vol. 68, no. 6, 2019.
- [32] J. Zhe et al., "Dissecting the NVIDIA volta GPU architecture via microbenchmarking.," *arXiv:1804.06826*, 2018.
- [33] M. Stefano et al., "Nvidia tensor core programmability, performance & precision.," *IEEE international parallel and distributed processing symposium workshops (IPDPSW)*, 2018.
- [34] G. Krishnan et al., "Interconnect-aware Area and Energy Optimization for In-Memory Acceleration of DNNs," *IEEE Design & Test*, vol. 37, no. 6, 2020.